Spectroscopic site determinations in erbium-doped lithium niobate

D. M. Gill
University of Wisconsin–Madison, Materials Science Program, Madison, Wisconsin 53706

L. McCaughan
University of Wisconsin–Madison, Electrical and Computer Engineering, Madison, Wisconsin 53706

J. C. Wright
University of Wisconsin–Madison, Chemistry Department, Madison, Wisconsin 53706
(Received 16 February 1995; revised manuscript received 31 July 1995)

Rare-earth (e.g., Er^{3+}, Nd^{3+}) based, guided wave optical amplification in lithium niobate ($LiNbO_3$) integrated optic systems is a new and important addition to the field of integrated optics. The application of total site selective spectroscopy to rare-earth-doped $LiNbO_3$ provides the most complete spectroscopic characterization of this class of materials to date. In a previous publication we identified six spectroscopic sites in Er:$LiNbO_3$ using total site selective spectroscopy, two of which are cluster sites which upconvert light using nonradiative energy transfer between Er ions within a given site. In this paper Er^{3+} site identifications are made based on a consideration of solid solution defect equations in conjunction with an experimental study of the site distribution as a function of dopant concentration (0.4–2.0 mol % Er:$LiNbO_3$) and the Li/Nb ratio in the crystal. The Li/Nb ratio was altered using a vapor phase equilibration technique. Our results indicate that increasing the Li_2O content of Er:$LiNbO_3$ not only reduces the cluster site concentration by ~30% but also increases the amount of light absorbed in the crystal by ~15%. This observation is, to the best of our knowledge, the first report of post growth materials processing in rare-earth-doped $LiNbO_3$ to effect a change in absorption or cluster site concentration. In addition, increasing the dopant concentration increases Li_2O deficiency in Er:$LiNbO_3$ crystals. Simple solid solution defect model calculations agree with these experimental results.

I. INTRODUCTION

$LiNbO_3$ is an active integrated optic host whose strong electroptic properties make possible guided wave signal modulation and switching,[1] quasiphase matched second harmonic generation,[2,3] and chirp compensation.[4] While the most sophisticated guided wave systems to date have been produced in $LiNbO_3$,[5] the technology has only recently incorporated monolithic optical gain.[6–10] Rare-earth doping (with Er^{3+} and Nd^{3+}) of $LiNbO_3$ has produced traveling-wave amplification, cw lasing, upconverting and self Q-switched lasers.[11] In addition, guided wave lasers have also been fabricated with monolithically integrated electro-optic intercavity elements.[12–15] These devices represent examples of a new class of miniaturized lasers/amplifiers which are based on a synergy of nonlinear optical properties and guided wave gain in lithium niobate. Er:$LiNbO_3$ devices are of particular interest because they operate at ~1.5–1.6 μm, a primary carrier wavelength region in telecommunications.[16]

Efforts to improve rare-earth-doped devices have predominantly focused on waveguide and cavity fabrication.[6–8,17,18] The materials engineering of the gain media itself is a potentially important aspect of device performance which, to date, has been generally neglected. Materials considerations are important because optical transitions utilized in these devices originate from forbidden transitions which are allowed in sites with nonspherically symmetric crystal fields. A transition's lifetime, cross section, and polarization are directly affected by an ion's microscopic environment. Maximizing the relative concentration of a specific site with a highly polarized or particularly large cross section, can help tailor a gain medium for optimal performance in a specific lasing geometry. In addition, the relative concentration of cluster sites, which can cause fluorescence quenching in optical telecommunications devices, has been modified in other crystal hosts via post growth processing.[19,20] Knowledge of the character and distribution of rare-earth sites in $LiNbO_3$ will not only aid in materials engineering but will also lend insight into new applications based in these media.

Site selective spectroscopy is a convenient and accurate method of determining relative changes in rare-earth site distributions within insulator hosts.[21] Unfortunately, the optical characterization of site distributions in rare-earth-doped $LiNbO_3$ is difficult because the broadening seen in fluorescence spectra, even at cryogenic temperatures (~12 K), is about as large as the separation between peaks from different sites.[22] Consequently, characterization using only standard site-selective spectroscopy yields incomplete results.[23,24] We recently demonstrated the optical characterization of site distributions in rare-earth-doped $LiNbO_3$ using the technique of *total* site selective spectroscopy.[22] Six sites were identified, two of which were cluster sites that upconvert light using a nonradiative energy-transfer process. These results represent the most complete optical site characterization of rare-earth-doped $LiNbO_3$ to date.

Previous work has focused on changing the Li/Nb ratio in doped $LiNbO_3$ to alter its site distributions.[23,25] Site determi-

 © 1996 The American Physical Society

nations can sometimes be made in rare-earth-doped crystals by altering the site distributions and correlating spectral features that change.[23,25] The stoichiometry of these crystals was varied by altering the concentrations of Li_2O and Nb_2O_5 in the melts from which they were grown. This method of materials engineering is not desirable for device fabrication because: crystals pulled from noncongruent melts have stoichiometric variations in the direction in which they are pulled; the amount of dopant (e.g., Cr^{3+}) incorporated in $LiNbO_3$ can vary by threefold with stoichiometry;[25] and it is difficult to grow large boules from noncongruent melts. An alternative method of altering crystal stoichiometry is vapor phase equilibration,[26–28] which produces crystals whose stoichiometry is homogeneously altered and whose dopant concentrations do not significantly vary from crystal to crystal. Therefore, vapor phase equilibrated crystals will allow one to determine changes in the crystal absorption due to the redistribution of rare-earth sites. In this paper we demonstrate the use of vapor phase equilibration to alter the stoichiometry of Er:$LiNbO_3$. Er site identifications are made based on spectroscopic site determinations made in Ref. 22 in conjunction with a consideration of solid solution defect equations and an experimental study of site redistributions as a function of both crystal concentration (0.4–2.0 mol % Er:$LiNbO_3$) and stoichiometry. Our results indicate that the site redistribution associated with bringing $LiNbO_3$ crystals closer to a stoichiometric composition may be useful for enhancing this material's performance as a gain medium.

II. EXPERIMENT

A. Concentration-dependent site distributions of Er in Er:$LiNbO_3$

Using the site determinations obtained from Ref. 22, standard site-selective spectroscopy was used to investigate changes in the relative site populations as a function of crystal concentration. Poled (single ferroelectric domain) Er:$LiNbO_3$ crystals were obtained from the Tianjin University, P. R. China, with Er concentrations of 0.2, 0.5, and 1.0 mol % Er_2O_3 (0.4, 1.0, 2.0 mol % Er:$LiNbO_3$, respectively). The crystal concentrations were verified using neutron activation analysis. The excitation beam was x propagating and linearly polarized at 45° to the y and z axes. Specific excitation and fluorescence transitions were used to determine the relative Er site distributions. Since the relative intensities of different scans were being compared, care was taken to normalize the fluorescence data with respect to shot-to-shot variations in pump power. Normalization was done by sampling a portion of the incident excitation beam and measuring its relative intensity using a pyroelectric detector and a gated integrator. Changes in fluorescence peak height then correspond to changes in the relative concentration of sites.

B. Vapor phase equilibration of Er:$LiNbO_3$

A poled (single ferroelectric domain), congruent (~48.6 at. % Li_2O and ~51.4 at. % Nd_2O_5), 1.0 mol % Er:$LiNbO_3$ crystal was brought closer to a stoichiometric composition (~50 at. % Li_2O and ~50 at. % Nd_2O_5) by the process of vapor phase equilibration.[26–28] To achieve this, a crucible and lid were made of lithium carbonate, Li_2CO_3, and niobium pentoxide, Nb_2O_5, powders in proportions such that the calcined end product was ~50% $LiNbO_3$ and ~50% Li_3NbO_4 by weight. The powders were mixed with ~20% carbo wax 4000 and pressed into molds with ~20 000 p.s.i. The carbo wax helps bind the precalcined powders and provides porosity to the post-calcined pieces which aids in mass transfer between the crucible and the Er:$LiNbO_3$. The pressed forms were dewaxed in an oven at 350 °C for 10 h, then calcined by first heating to 1000 °C for 10 h and then 1100 °C for 1 h. A 1.5 mm×1 cm×1 cm congruent crystal was wrapped with platinum wire to avoid contact between the crucible and sample, placed into the two-phase crucible, and heated to 1050 °C for ~150 h (heating rate ~150 C/h, cooling rate ~400 C/h). At 1050 °C the crucible out gasses Li_2O which is taken up by the Er:$LiNbO_3$ and the congruent crystal is brought closer to a stoichiometric composition. The geometry of the crucible and crystal was such that the crystal was no more than 6 mm from any inner wall to facilitate mass transfer of Li_2O from the crucible to the Er:$LiNbO_3$ crystal.[26] When the crystal was removed from the crucible there were a large number of internal cracks close to its x-y crystallographic plane. These cracks were likely caused either by inadvertent rapid heating/cooling or by strains induced by stoichiometric variations along the length of the crystal. Cracks often occur in heated $LiNbO_3$ crystals which have large compositional inhomogeneities along their length. Fluorescence measurements were taken with the excitation beam y propagating and linearly polarized to a 45° angle between the x and z axis.

III. THEORY

A. Fluorescence transient lifetime

There are two fundamental assumptions which are typically considered before forming rate equations for fitting fluorescence transients. Namely, whether the fluorescence is coming from ions which are relaxing independently (single ion sites) or from relaxations which involve energy transfer between ions in proximity to each other (cluster sites). The rate equations associated with these two processes are distinctly different. The cluster sites have additional energy states available as a result of nonradiative energy transfer between ions within the site. In order to fit the nonupconverted transients it is assumed that the contribution from the cluster sites is small compared to that of the other Er sites in $LiNbO_3$. This assumption is justified by the fact that fluorescence transients measured from levels that are lower in energy than the one being pumped (and thus were not dependent on upconversion) displayed time dependencies dominated by single ion relaxation characteristics [Fig. 1(a)]. The nonupconverted fluorescence transients could be fit best by assuming that nonradiative multiphonon relaxation between successive levels was the dominant means of populating lower crystal-field levels. The rate equations associated with single ion relaxations in a four-level system are

$$dN_4/dt = -w_4N_4, \tag{1}$$

$$dN_3/dt = \phi_{43}w_4N_4 - w_3N_3, \tag{2}$$

$$dN_2/dt = \phi_{32}w_3N_3 - w_2N_2, \tag{3}$$

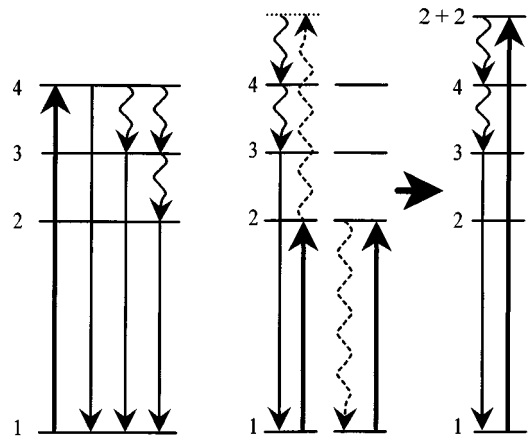

FIG. 1. Schematic diagram of energy manifolds in rare-earth ions. The left side of the picture represents single ion relaxations in an excited rare-earth ion. The middle portion of the figure gives an example of a possible dimer site relaxation which involves upconversion via nonradiative energy transfer between the rare-earth ions within the dimer. The right side of the figure shows the same relaxation process, however, the two ions within the dimer site are considered as a single fluorescing element. The straight arrows represent radiative transitions, the solid-wavy arrows represent phonon assisted nonradiative transitions, the dotted-wavy arrows represent energy transfer processes, and the dotted manifold level represents a virtual energy level which is present due to the interaction between the ions within the dimer.

where ϕ_{ij} is the branching ratio for nonradiative relaxations from level i to level j. These equations assume that level 3 is only populated by direct nonradiative relaxations from level 4. In turn, level 2 is only populated by nonradiative relaxations from level 3. Relaxations from level 4 directly to level 2 are ignored. It is also assumed that the population N_4 is created instantaneously by the excitation pulse. Solutions to these equations are given by

$$N_4 = N_4^0 \exp(-w_4 t), \tag{4}$$

$$N_3 = \phi_{43} N_4^0 w_4 (w_3 - w_4)^{-1} [\exp(-w_4 t) - \exp(-w_3 t)], \tag{5}$$

$$N_2 = \phi_{43}\phi_{32} N_4^0 w_4 w_3 [(w_2 - w_3)(w_4 - w_3)(w_2 - w_4)]^{-1} \times [(w_4 - w_3)\exp(-w_2 t) + (w_2 - w_4)\exp(-w_3 t) + (w_3 - w_2)\exp(-w_4 t)]. \tag{6}$$

Upconverted fluorescence transients could be fit best by assuming that nonradiative energy transfer, rather than excited state absorption, was the dominant upconverting mechanism. Er cluster sites are assumed to exist as Er ion pairs, referred to as a dimer site. A dimer is considered as a single fluorescing element [Fig. 1(b)].[29] The excited dimer population is labeled as N_d and represents the number of dimers in which both ions are excited as a result of an excitation pulse. The two ions within the dimer are labeled "a" and "b". It is assumed that there are three ways for the dimers to be depopulated: by the independent relaxation of ion a via nonupconverting mechanisms, the independent relaxation of ion b via nonupconverting mechanisms, or by upconversion between ions a and b. The rate equations are as follows:

$$dN_d/dt = -(N_d w_a + N_d w_b + N_d w_u) = -N_d(w_a + w_b + w_u) = -N_d w_d, \tag{7}$$

where w_a (w_b) is the relaxation rate of ion a (b) in the dimer pair without considering upconversion, w_u is the rate of dimer depopulation caused by upconversion and w_d is the rate of depopulation of the excited dimer. The upper state population is given by

$$dN_3/dt = w_u N_d - w_3 N_3, \tag{8}$$

where w_3 is the intrinsic decay rate of level 3. The solution of these equations gives

$$N_3 = \frac{N_d^0 w_u}{[w_3 - (w_a + w_b + w_u)]} \{\exp[-(w_a + w_b + w_u)t] - \exp(-w_3 t)\}. \tag{9}$$

This result is applied to upconverted fluorescence transients in Sec. IV B.

B. Defect modeling

In this section, solid solution defect equations for Er:$LiNbO_3$ are considered. In doing so, the intrinsic equations (solid solution defect equations in the absence of Er) are formed with the addition of Er as a charged defect. Defects are assumed to have a constant free energy of formation within the range of dopant concentrations considered. In addition, charge compensation by free electrons is ignored. Before dealing with the mass and charge balance equations some important points will be discussed from related work.

Czochralski growth of Er:$LiNbO_3$, and $LiNbO_3$,[30] produces Li_2O deficient single crystal material with a congruent composition, ~48.6% Li_2O.[31] The most common defect structure associated with the compensation for Li_2O deficiency in undoped crystals has been shown to be Nb_{Li^4},[32] using Kroger-Vink notation.[33] This defect exists at a concentration of ~5.9% in the crystal, and is present in an associated defect complex with the defect $V_{Nb^{5'}}$ in a concentration such that $4[Nb_{Li^4}] = 5[V_{Nb^{5'}}]$.[32,34] This defect complex is thought to exist within regions of an illmenitelike intergrowth present within the perfect $LiNbO_3$.[35,36] The oxygen sublattice is found to be filled in undoped $LiNbO_3$.[31] These results have led previously proposed models to focus on defects exclusively on the cation sublattice.[28,32,35–38] Computer modeling of $LiNbO_3$ indicates that Li Frenkel disorder, "$LiNbO_3$" $\leftrightarrow V_{Li'} + Li_I$, is a relatively favored intrinsic defect. Nb Frenkel disorder, "$LiNbO_3$" $\leftrightarrow V_{Nb^{5'}} + Nb_{I^5}$, and O Frenkel disorder, "$LiNbO_3$" $\leftrightarrow V_{O^{2.}} + O_{I^{2'}}$, are not favored.[34] In addition, experiments using a Rutherford backscattering technique on ~0.25 mol % Eu:$LiNbO_3$ found that Eu^{3+} ions exclusively substitute at Li and Nb lattice locations. No interstitial ions were found.[39]

In order to model the site distribution as a function of stoichiometry and dopant concentration a generalized model for the defect system is necessary. A system of defect equilibrium equations is developed with the defect concentrations

regarded as unknowns. We assume there is no defect-defect interaction. There is concern about this assumption because of the high concentration of intrinsic defects found even in undoped crystals. However, to consider such interactions would require a much more complicated modeling technique. Other researchers have applied more complicated models to $LiNbO_3$ systems.[35–37]

The stoichiometry is defined by

$$(1+\alpha)AX_{1/2}(1+\beta)BX_{5/2}(\Delta)RX_{3/2} = R_{\Delta}:A_{(1+\alpha)}B_{(1+\beta)}X_{(3+\alpha/2+5\beta/2+3\Delta/2)}, \quad (10)$$

where, for our case, A=Li, B=Nb, X=O, and R=Er. This equation indicates that we are dealing with the four constituents as a ternary mixture of oxides. The equations defining material balance are

$$1+\alpha=[A_A]+[A_B]+[A_I], \quad (11)$$

$$1+\beta=[B_B]+[B_A]+[B_I], \quad (12)$$

$$3+\alpha/2+5\beta/2+3\Delta/2=[X_X]+[X_I], \quad (13)$$

$$\Delta=[R_A]+[R_B]+[R_I], \quad (14)$$

where $[A_B]$ represents the probability of an A ion being on a B lattice location, $[A_I]$ represents the probability of an A ion being in an interstitial location. Δ represents the Er concentration and α and β represent mol % deviations from stoichiometry of the Li and Nb concentrations, respectively. The site balance equations are

$$[A_A]+[B_A]+[V_A]+[R_A]=1, \quad (15)$$

$$[B_B]+[A_B]+[V_B]+[R_B]=1, \quad (16)$$

$$[X_X]+[X_V]=3, \quad (17)$$

assuming the crystal is in a 1:1:3=Li:Nb:O phase. The defect equilibrium and mass action equations are given by

$$A_A=A_I+V_A \Rightarrow \frac{[A_I][V_A]}{[A_A]}=K1, \quad (18)$$

$$B_B=B_I+V_B \Rightarrow \frac{[B_I][V_B]}{[B_B]}=K2, \quad (19)$$

$$A_B=A_I+V_B \Rightarrow \frac{[A_I][V_B]}{[A_B]}=K3, \quad (20)$$

$$B_A=B_I+V_A \Rightarrow \frac{[B_I][V_A]}{[B_A]}=K4, \quad (21)$$

$$X_X=X_I+V_X \Rightarrow \frac{[X_I][V_X]}{[X_X]}=K5, \quad (22)$$

$$R_A=R_I+V_A \Rightarrow \frac{[R_I][V_A]}{[R_A]}=K6, \quad (23)$$

$$R_B=R_I+V_B \Rightarrow \frac{[R_I][V_B]}{[R_B]}=K7. \quad (24)$$

We will assume that the crystal accommodates the incorporation of Er by changes in the cation sublattice only. This assumption is based on the fact that we saw no evidence of F-center defects in Er:$LiNbO_3$ since their characteristic optical absorption bands are absent.[40] In addition, computer modeling of dopant incorporation in $LiNbO_3$ indicates that O_I are not energetically favored defects.[37] Since the equations involving X_X, V_X, and X_I [Eqs. (13), (17), and (22)] are independent of the other 11 equations, the equations can be solved as one group of three and one group of 11 independent equations and unknowns. A final independent equation and unknown are introduced to the system of 11 by considering charge balance,

$$[V_A^-]+5[V_B^{5-}]+4[A_B^{4-}]+2[R_B^{2-}] = [A_I^+]+5[B_I^{5+}]+3[R_I^{3+}]+2[R_A^{2+}]+4[B_A^{4+}]. \quad (25)$$

The imposition of charge balance brings the need for a new dependent variable. We therefore assume that α, β, and Δ are not independent of each other. This assumption is reasonable since it has been reported that the amount of a dopant taken up by a $LiNbO_3$ crystal, grown from a melt, can vary by as much as threefold with variations in the Li/Nb ratio of the melt (i.e., variations in the crystal stoichiometry).[25] In our calculations one of these three quantities was taken as an independent variable, one as a dependent variable and the other held constant. For example, in model calculations in which the dopant concentration (Δ) was used as an independent variable, we assumed β to be a known constant and α to be a new unknown [since Li_2O is much more volatile than Nb_2O_5 (Ref. 41)]. This system of 12 equations can be reduced to the following four equations and four unknowns defined in terms of the unknowns α, A_I, B_I, and R_I:

$$1+\alpha=\frac{[A_I]/K1}{[A_I]/K1+[B_I]/K4+[R_I]/K6+1}+\frac{[A_I]/K3}{[B_I]/K2+[A_I]/K3+[R_I]/K7+1}+[A_I], \quad (26)$$

$$1+\beta=\frac{[B_I]/K4}{[A_I]/K1+[B_I]/K4+[R_I]/K6+1}+\frac{[B_I]/K2}{[B_I]/K2+[A_I]/K3+[R_I]/K7+1}+[B_I], \quad (27)$$

$$\Delta=\frac{[R_I]/K6}{[A_I]/K1+[B_I]/K4+[R_I]/K6+1}+\frac{[R_I]/K7}{[B_I]/K2+[A_I]/K3+[R_I]/K7+1}+[R_I], \quad (28)$$

TABLE I. Wavelengths of the transition peaks for the sites identified in Ref. 22. Values are given in angstroms.

	Line *a*	Line *b*	Line *c*	Line *d*	Line *e*
Site 1 λ (Å)	6514.4	6521.5	6557.8	6584.3	6600.9
Site 2 λ (Å)	6512.5	6523.6	6556.6	6584.2	6599.6
Site 3 λ (Å)	6506.4	6515.8	6552.5	6582.2	6598.4
Site 4 λ (Å)	6506.8	6518.6	6553.2	6579.1	6596.8
Site 5 λ (Å)	6504.1	6512.9	6551.3	6578.1	6596.1
Site 6 λ (Å)	6501.1	6508.6	6549.0	6574.0	6592.7

$$\frac{1}{[A_I]/K1+[B_I]/K4+[R_I]/K6+1}+\frac{1}{[B_I]/K2+[A_I]/K3+[R_I]/K7+1}\left(5+\frac{4[A_I]}{K3}+\frac{2[R_I]}{K7}\right)$$
$$=[A_I]+5[B_I]+3[R_I]+\frac{2[R_I]/K6}{[A_I]/K1+[B_I]/K4+[R_I]/K6+1}+\frac{4[B_I]/K4}{[A_I]/K1+[B_I]/K4+[R_I]/K6+1}. \quad (29)$$

Each term within these equations represents a specific defect probability of occurrence. Equations (26)–(29) are equal term-by-term to Eqs. (11), (12), (14), and (25), respectively.

This system of four equations and four unknowns can be solved by assuming values for the constants $K1-K7$. These values are determined by assigning probabilities of occurrence for each defect in the crystal (Sec. IV C). It is assumed that the Er concentration is low and the intrinsic defect concentrations remain relatively unchanged by doping the pure $LiNbO_3$ with small Er concentrations. The equations were solved numerically after estimating defect concentrations according to the review at the beginning of this section. Those defects with low concentrations were neglected in the numerical solutions. This is effectively assuming that the dominant defects associated with charge compensation for dopant ions in $LiNbO_3$ are the V_{Nb} and Nb_{Li} defects. This has also been suggested by other researchers for dopant levels of less than a few percent.[28,38]

IV. RESULTS

A. Spectroscopy

The wavelengths corresponding to the transitions between the five $^4F_{9/2}$ manifold levels and the bottom level of the $^4I_{15/2}$ (ground state) manifold are listed in Table I for the six sites in Er:$LiNbO_3$.[22] Lifetime measurements from the transition wavelengths in Table I are listed in Table II. In Ref. 22 we classified the six sites in Er:$LiNbO_3$ into three groups based on the absorption and emission characteristics of the various sites. We found two single ion (nonclustered) site groups, namely, sites 1&2, and sites 3&4 (as labeled in Ref. 22). We also assigned sites 5 and 6 as Er cluster sites. Sites 1–4 were found to be major sites while sites 5&6 seemed to be lower in concentration. The lifetime differences shown in Table II are consistent with the classifications summarized above from Ref. 22.

TABLE II. Measured lifetimes from the transition wavelengths listed in Table I. Values are given in microseconds.

	Line *a*	Line *b*	Line *c*	Line *d*
Site 1 (μs)	1.7	1.7	1.7	1.7
Site 2 (μs)	1.7	1.7	1.7	1.7
Site 3 (μs)	1.5	1.55	1.55	1.7
Site 4 (μs)	1.6	1.57	1.56	1.6
Site 5 (μs)	1.55	1.55	1.58	1.58
Site 6 (μs)	1.65	1.7	1.65	1.55

Sites 5 and 6 are assigned to clustering since only these sites produced upconverted light when pumping the $^4F_{9/2}$ manifold (~650 nm). Upconverted light was observed from the $^2P_{3/2}\rightarrow{}^4I_{13/2}$ (~475 nm), $^4G_{11/2}\rightarrow{}^4I_{15/2}$ (~388 nm), $^2H_{9/2}\rightarrow{}^4I_{15/2}$ (~412 nm), and $^4S_{3/2}\rightarrow{}^4I_{15/2}$ (~540 nm) transitions. Upconversion can arise from two possible processes, excited-state absorption and/or nonradiative energy transfer.[19,20] From a materials engineering point of view, the distinction between these two processes is significant. Excited-state absorption in any medium is a fundamental consequence of a given pump/signal choice; as a result it is not easily altered. In contrast, nonradiative energy transfer arises from a distinct subset of the total Er^{3+} population, namely cluster sites, and can be enhanced or suppressed by changing the relative concentration of these sites.[19,20] We assign the dominant upconverting mechanism in sites 5 and 6 to energy transfer between two excited Er ions that are clustered. The alternate mechanism, a sequential two-step absorption (excited state absorption), is unlikely for the following reasons: upconversion is not observed for the major sites (1–4) despite the similarity of their electronic states to the upconverting sites; and the quantitative fittings we have made of fluorescence transient kinetics are consistent with energy transfer but not with sequential absorption (see Sec. IV B).[29] In addition, Fig. 2 shows the crystal-field manifolds for a single Er ion and a cluster site. The cluster site has more electronic states available due to energy transfer between the ions within the dimer. The energy of two excitation photons $[2(^4F_{9/2})]$ is also shown in Fig. 2 to simulate excited-state absorption in single ion sites. Figure 2 shows that there are no absorbing levels at the wavelength required for a sequential absorption of the 5 ns pulse. This result is specific to

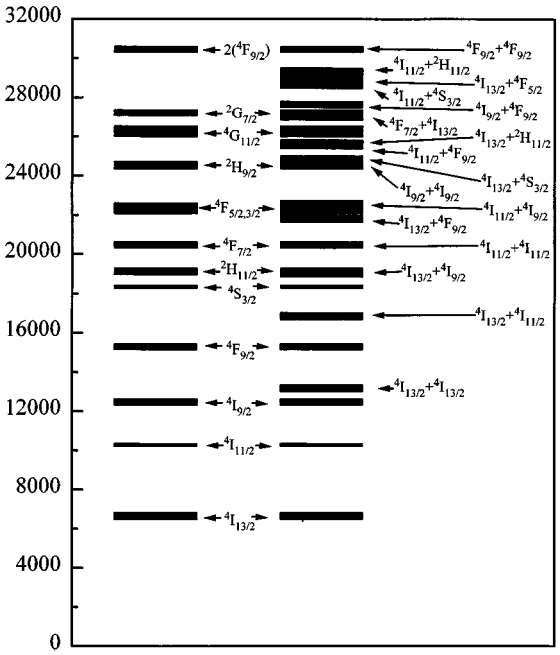

FIG. 2. Diagram of the manifold transition energies in Er:$LiNbO_3$. The left side of the figure shows the single ion electronic states, and the right side of the figure shows the dimer site electronic states. The additional energy states in the dimer sites are made available through energy transfer between ions within the dimer.

pumping the $^4F_{9/2}$ manifold at low temperatures. A given manifold which has levels that are more accessible for excited state absorption, for example the $^4I_{9/2}$ manifold for the $^4I_{13/2}$ (~1480 nm) excitation, the $^4F_{7/2}$ manifold for the $^4I_{11/2}$ (~980 nm) excitation or the $^2H_{9/2}$ manifold for the $^4I_{9/2}$ (~810 nm) excitation (Fig. 2), will have stronger contributions to the upconverted fluorescence via this alternate mechanism.

Relatively strong upconversion is also seen when exciting the $^4S_{3/2}$ manifold (~540 nm). If the $^4F_{7/2}$, $^4F_{5/2}$ or $^4F_{3/2}$ manifolds are excited, comparatively weak upconversion is seen. Quantitative fittings of the radiative decay transients not only indicate that upconversion from these four levels is predominantly caused by nonradiative energy transfer [Eq. (9)], but also that the energy-transfer process is originating from the $^4S_{3/2}$ manifold regardless of whether the $^4S_{3/2}$, $^4F_{7/2}$, $^4F_{5/2}$ or $^4F_{3/2}$ manifold is excited. Complementary total site selective scans of upconverted and nonupconverted fluorescence obtained while pumping the $^4S_{3/2}$ manifold are shown in Figs. 3(a) and 3(b). Correlations between upconverted and nonupconverted spectra can be made by comparing these two plots. Figures 3(a) and 3(b) show that the mean $^4S_{3/2}$ energy is red shifted for the dimer sites just as observed for the $^4F_{9/2}$ excitation experiments (Ref. 22). Figure 3(b) also shows that the two dimer sites are not resolved when exciting the $^4S_{3/2}$ manifold. However, this result is not surprising since the spectrum shown in Fig. 3(a) shows that even the major nonupconverting sites cannot be resolved when exciting the $^4S_{3/2}$ manifold.

B. Lifetime determinations

Table III(a) is a listing of the lifetimes found for the various crystal-field transitions in a 1.0 mol % Er:$LiNbO_3$ crystal. Table III(b) shows the rise and fall times of the transients collected. There is a range of lifetimes reported because the transients show a continuous shift from one lifetime to an other as one tunes the excitation and fluorescence wavelengths from one site to another through the inhomogeneous distribution.

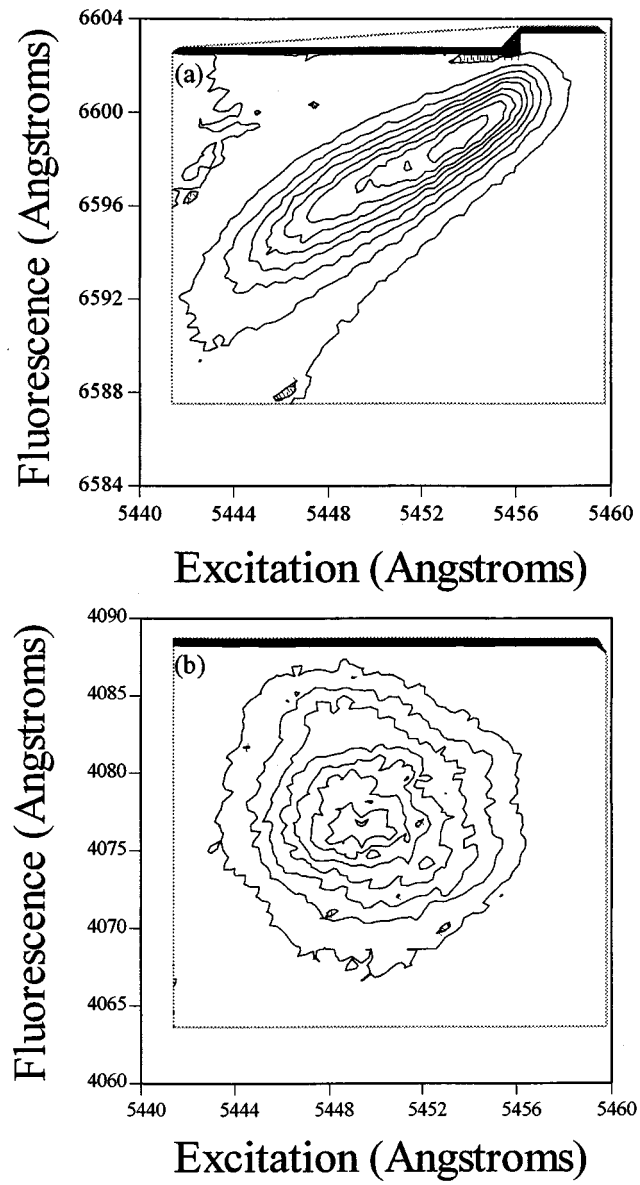

FIG. 3. (a) Total site-selective contour plot of fluorescence from the $^4F_{9/2}\rightarrow{}^4I_{15/2}$ transition while exciting to the $^4S_{3/2}$ manifold with a x-propagating, pulsed (~5 ns), and unpolarized excitation beam. (Excitation line width ~0.4 Å; fluorescence resolution ~0.5 Å). (b) Total site-selective contour plot of upconverted fluorescence from the $^2P_{3/2}\rightarrow{}^4I_{13/2}$ transition while exciting the $^4S_{3/2}$ manifold. The excitation beam was x propagating, pulsed (~5 ns) and unpolarized. (Excitation line width ~0.4 Å; fluorescence resolution ~3 Å).

To quantitatively apply the rate equations associated with the dimer sites (Sec. III A), some transition lifetimes from the individual ions must be known. Direct measurement is difficult since the cluster sites are minor sites. Excitation capabilities were limited to the ~650, ~540, ~475, and ~450 nm manifolds ($^4F_{9/2}$, $^4S_{3/2}$, $^4F_{7/2}$, $^4F_{5/2}$, and $^4F_{3/2}$ mani-

TABLE III. (a) Measured lifetimes from a 1.0 mol % Er:$LiNbO_3$ crystal. (b) Rise and fall times of the transients collected from the listed transitions.

(a)

Fluorescence state	Wavelength (nm)	Lifetime (μs)
$^2P_{3/2}$	323	10–12
$^2H_{9/2}$	410	0.5
$^4S_{3/2}$	540	15–110
$^4F_{9/2}$	650	1.8–4
$^4I_{9/2}$	810	0.25
$^4I_{11/2}$	980	300–320

(b)

Pump level	$^4I_{11/2}$ 980 nm	$^4I_{9/2}$ 820 nm	$^4F_{9/2}$ 650 nm	$^4S_{3/2}$ 540 nm	$^4S_{3/2}$ 852 nm	$^2P_{3/2}$ 475 nm	$^2H_{9/2}$ 412 nm	$^2P_{3/2}$ 407 nm	$^2P_{3/2}$ 323 nm
$^4F_{5/2}$		2.5	2		0.2			12	
450 nm		35	32–36		40			22	
$^4F_{7/2}$	35–40	2	1.8–2	0.1	0.1			12	
490 nm	300	37	35–38	35	35			22	
$^4S_{3/2}$	35	2–5	1.8–4	0.1		10		10	12
540 nm	300	19–30	20–37	15–40		20		22	22
$^4F_{9/2}$	2	0.25	0.1	1.5–2		2	0.4		
650 nm	300	1.8–2	1.6–1.8	20–110		10	0.5		

folds, respectively). Strong upconversion was only seen when pumping the ~650 and ~540 nm lines. Since fluorescence from the nonclustered sites dominated the nonupconverted fluorescence, lifetimes from the cluster site $^4F_{9/2}$ level could not be reliably measured. Lifetimes for the $^4S_{3/2}$ level were determined by assuming values for the $^4F_{9/2}$ manifolds and fitting the upconverted $^4S_{3/2}$ transients. This assumption is justified by the large difference between the lifetimes of the $^4F_{9/2}$ and $^4S_{3/2}$ cluster manifolds (Table III). The upconverted $^4S_{3/2}$ fluorescence transients from the two dimer sites were best fit using lifetimes of 20 and 110 μs for sites 5 and 6, respectively. In order to fit the fluorescence transients produced when both dimer sites were being excited, Eq. (9) must include the relaxation rates from both dimers:

$$N_3=\frac{N_d^0 w_u^{(5)}}{[w_3^{(5)}-(w_a^{(5)}+w_b^{(5)}+w_u^{(5)})]}\{\exp[-(w_a^{(5)}+w_b^{(5)}+w_u^{(5)})t]-\exp(-w_3^{(5)}t)\}+\frac{N_d^0 w_u^{(6)}}{[w_3^{(6)}-(w_a^{(6)}+w_b^{(6)}+w_u^{(6)})]}\times\{\exp[-(w_a^{(6)}+w_b^{(6)}+w_u^{(6)})t]-\exp(-w_3^{(6)}t)\}. \tag{30}$$

Here $w_3^{(5)}$ and $w_3^{(6)}$ are the decay rates of the $^4S_{3/2}$ manifolds in the dimer sites 5 and 6, respectively, without upconversion. While lifetimes for the dimer $^4S_{3/2}$ manifolds can be measured, the transition lifetimes of the individual ions within the dimer could not be resolved, precluding the determination of energy transfer rates within the dimer. The cluster sites labeled 5 and 6 could not be resolved when exciting the $^4S_{3/2}$ manifold while collecting upconverted fluorescence. Consequently, the upconverted $^2P_{3/2}$ fluorescence transients collected while exciting the $^4S_{3/2}$ manifold were fit with Eq. (9) (Table III).

The upconverted $^2H_{9/2}$ fluorescence collected while pumping the $^4F_{9/2}$ state is very weak. This transient has a very fast rise and fall time (Table III). The lifetime of the pair state which produces the upconverted $^2H_{9/2}$ fluorescence is much faster than that of the pair state which produces the upconverted $^4S_{3/2}$ fluorescence, even though the same manifold is being excited. Therefore, the fluorescence associated with these two transitions is either coming from different processes or different sites. The $^2P_{3/2}\rightarrow{}^4I_{11/2}$ transition fluorescence (475 nm) collected while exciting the $^4F_{9/2}$ manifold is also surprising because the $^4F_{9/2}-{}^4F_{9/2}$ pair state is lower in energy than the $^2P_{3/2}$ state. Since the sample is at ~12 K it is unlikely that the dimer is absorbing phonons from the lattice to produce this signal. This signal could be originating from three-body energy transfer in higher-order cluster sites.

TABLE IV. Defect concentrations as predicted by our model. The numbers given represent the probability of occurrence for each defect. (a) The Er concentration (Δ) is taken as the independent variable, the Li_2O content (α) is the dependent variable and the Nb_2O_5 content (β) is assumed to remain constant. (b) The Li_2O content (α) is the independent variable, the Nb_2O_5 content (β) is the dependent variable and the Er concentration (Δ) is assumed to remain constant. (c) Same as (b) but with a higher Er concentration.

Δ	α	β	Er_{Li}	Er_{Nb}	Li_{Li}	Nb_{Nb}	Li_{Nb}	Nb_{Li}	V_{Li}	V_{Nb}	Li_I	Nb_I	Er_I
							(a)						
0.001	−0.0579	0.010 98	0.000 49	0.000 31	0.942	0.955	1.05×10^{-6}	0.0575	0.000 09	0.046	0.000 1	1.05×10^{-9}	5.3×10^{-10}
0.002	−0.0609	0.010 98	0.001	0.001	0.939	0.951	1.00×10^{-6}	0.0599	0.000 1	0.048	0.000 1	1.00×10^{-9}	1.00×10^{-9}
0.005	−0.07	0.010 98	0.002 65	0.002 35	0.930	0.944	8.76×10^{-7}	0.0673	0.000 13	0.054	0.000 08	8.8×10^{-10}	2.09×10^{-9}
0.01	−0.0851	0.010 97	0.005 74	0.004 26	0.915	0.933	7.23×10^{-7}	0.0792	0.000 18	0.064	0.000 05	7.4×10^{-10}	3.20×10^{-9}
0.02	−0.1152	0.010 96	0.012 81	0.007 19	0.885	0.909	5.29×10^{-7}	0.1021	0.000 31	0.084	0.000 03	5.5×10^{-10}	4.11×10^{-9}
							(b)						
0.002	−0.0398	0.0068	0.000 78	0.001 22	0.960	0.968	1.59×10^{-6}	0.0392	0.000 04	0.031	0.000 24	1.57×10^{-9}	1.87×10^{-9}
0.002	−0.0609	0.010 98	0.001	0.001	0.939	0.951	1.00×10^{-6}	0.0599	0.000 1	0.048	0.000 1	1.00×10^{-9}	1.00×10^{-9}
0.002	−0.0800	0.014 78	0.001 14	0.000 86	0.920	0.935	7.34×10^{-7}	0.0788	0.000 18	0.063	0.000 06	7.5×10^{-10}	6.5×10^{-10}
							(c)						
0.01	−0.0397	0.002	0.003 73	0.006 27	0.960	0.966	1.72×10^{-6}	0.036	0.000 03	0.028	0.000 29	1.74×10^{-9}	1.07×10^{-8}
0.01	−0.0600	0.006	0.004 79	0.005 21	0.940	0.951	1.09×10^{-6}	0.055	0.000 08	0.044	0.000 12	1.09×10^{-9}	5.68×10^{-9}
0.01	−0.0800	0.009 98	0.005 57	0.004 42	0.920	0.936	7.78×10^{-7}	0.074	0.000 16	0.060	0.000 06	7.9×10^{-10}	3.54×10^{-9}
0.01	−0.0851	0.010 98	0.005 74	0.004 26	0.915	0.932	7.23×10^{-7}	0.079	0.000 18	0.064	0.000 05	7.4×10^{-10}	3.20×10^{-9}

C. Model calculations

Results from the solution of Eqs. (28)–(31) are shown in Tables IVa–IVc. The model predicts that at low dopant levels the change in Er site distributions as a function of dopant concentration is very small. This insensitivity occurs because at relatively low Er concentrations (<0.5 mol %) the dopant has little effect on the intrinsic defect populations which are in a concentration of ~5% (assuming the dopant ions are charge compensated predominantly by the intrinsic defects Nb_{Li} and V_{Nb}, Sec. III B).[38,40] As the dopant levels are increased in the model, the incorporation of the Er starts to shift the intrinsic defect concentrations. This shift changes the probability of Er_{Li} and Er_{Nb} site formation. Table IVa indicates that if β is held constant (where β is the Nb deviation from stoichiometry) and the dopant levels are increased, there is an increase in both Li_2O deficiency and the relative Er_{Li} site population. Alternatively, as the crystal is brought closer to stoichiometry and the dopant level is held constant (Tables IVb and IVc), the model predicts an increase in the relative concentration of Er_{Nb} sites. The general trend seen in this simple model is that increasing the dopant concentration and increasing the Li_2O content have opposite effects on the site distribution in the crystal. These model calculations are compared to spectroscopic measurements below.

D. The redistribution of Er sites as a function of Er concentration

Site-selective spectroscopy was used to detect the change in the relative site distributions between the 0.4, 1.0, and 2.0 mol % Er:$LiNbO_3$ crystals (Table V). The site distributions are determined by measuring the fluorescence intensity from a selected transition in six different sites. The six measured values are added and the relative contribution from each site is defined as its relative site concentration. The most striking result is that the proportion of cluster sites, for example site 6, relative to the single ion sites increases in an approximately linear manner with an increase in the Er concentra-

TABLE V. Percent changes in the relative site concentrations between 0.4 and 1.0 mol % Er:$LiNbO_3$ crystals and 0.4 and 2.0 mol % Er:$LiNbO_3$ crystals.

Site number as identified in Ref. 22	Percent change between 0.4 and 1.0 mol % Er:$LiNbO_3$	Percent change between 0.4 and 2.0 mol % Er:$LiNbO_3$
1	−1	−24
2	−4	−7
3	−15	−28
4	−2	+11
5	+5	+16
6	+68	+158

TABLE VI. Percent changes in the relative site concentrations as a function of Er concentration and Li/Nb stoichiometry of the 1&2 and 3&4 site groups. Contributions from the dimer sites are ignored.

	Relative change between a 0.4 and 2.0 mol % crystal	Relative change between a congruent and VPE crystal
1&2 site group	−2.8%	+20.8
3&4 site group	+3.6%	−9.0

tion for the crystals studied (Table V). This increase is consistent with the dependence expected for dimer clusters.[42] While the concentration of site 5, the second cluster site, also increases with concentration, it does so more slowly. This difference is probably caused by the spectral overlap between sites 4 and 5 (there is minimal overlap between site 6 and any other site). Closer inspection of the data in Table V shows that the relative concentration of the major sites (1–4) do not significantly change between Er concentrations of 0.4 and 1.0 mol %. There is a small reduction in the relative concentration of site 3, but this change is near the error limit of our system (~15%). Larger changes in the site distributions are seen if the 0.4 and 2.0 mol % Er:$LiNbO_3$ crystals are compared. These results are also consistent with our modeling results.

Changes in the relative proportion of the Er sites were determined by considering the three groups of Er sites previously discussed in Sec. IV A (sites 1&2, 3&4, and 5&6). We further assume that the Er^{3+} ions exclusively substitute at Li and Nb lattice locations, as has been shown for Eu^{3+} in Eu:$LiNbO_3$.[39] We suggest that one pair of similar single ion sites (sites 1–4 are identified as the single ion sites) represents Er ions in two different Li sites and the other pair represents Er ions in two Nb sites. The dimer sites (sites 5&6) are assumed to be predominantly composed of one Er_{Li} and one Er_{Nb}. This self-charge compensating scenario produces a neutral defect which contributes equal numbers of Er_{Li} and Er_{Nb} sites to the total population. Therefore, when determining the changes in the Er_{Li} and Er_{Nb} site populations, the contributions from the dimer sites are ignored.

Table VI shows the changes in the Er site groups as a function of concentration. A slight increase in the relative concentration of sites 3&4 over sites 1&2 is seen with an increase in Er concentration. Since the modeling indicates an increase in Er_{Li} sites with an increase in Er concentration, we assign the 3&4 site group as Er_{Li} sites. There is still insufficient evidence to make this assignment definitive. However, these results are consistent with the redistribution of Er sites associated with changes in the crystal stoichiometry discussed in the next section.

E. The redistribution of Er sites as a function of Li/Nb stoichiometry

Figure 4 shows normalized low-temperature (~12 K) absorption scans of the $^4F_{9/2}$ manifold from an untreated (congruent) Er:$LiNbO_3$ crystal (~48.6% Li_2O and ~51.4% Nb_2O_5) and a crystal which was vapor phase equilibrated

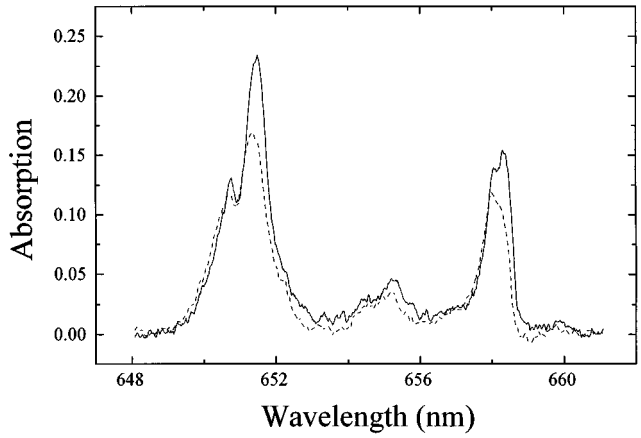

FIG. 4. Low-temperature (~12 K) absorption scans of the $^4F_{9/2}$ manifold in Er:$LiNbO_3$ for a congruent crystal (dashed line) and a crystal brought closer to a stoichiometric composition using vapor phase equilibration (solid line). (Monochromator resolution ~0.4 nm.)

toward a more stoichiometric composition. The scans show two distinct results: a redistribution in the relative concentrations of the spectroscopic sites (shown by a change in the shape of the spectrally dependent absorption) and ~15% increase in the amount of light absorbed by the total Er population in the treated crystal (determined by comparing the areas under each curve). This figure also shows a 35% increase in the low-temperature absorption cross section at 651.5 nm in the treated crystal. Low-temperature excitation scans of individual sites also showed a 10% narrowing of the absorption lines as a result of the vapor phase equilibration toward stoichiometry. The linewidth is a measure of the degree of variation between ions in similar sites. The narrowing in the linewidth is an indication that the inhomogeneous broadening is reduced in the treated crystal. Room-temperature absorption scans, Fig. 5, also show an increase in the amount of light absorbed by the treated crystal.

The measured site redistribution (as indicated by changes in fluorescence peak heights) caused by the vapor phase

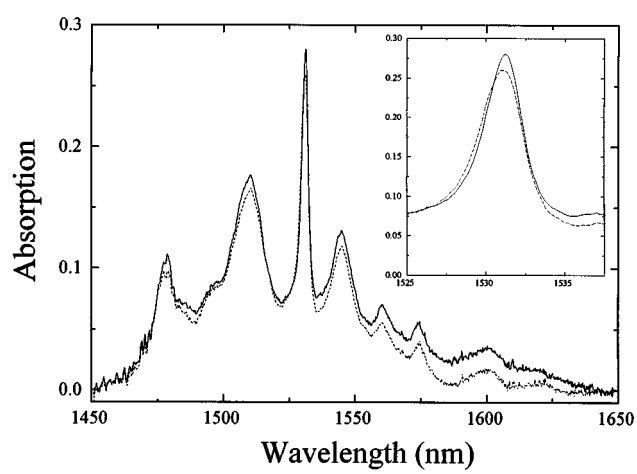

FIG. 5. Room-temperature absorption scans of the $^4I_{15/2}$ manifold in Er:$LiNbO_3$ for a congruent crystal (dashed line) and a crystal brought closer to a stoichiometric composition using vapor phase equilibration (solid line). The inset shows an expanded view of the 1531 nm transition.

TABLE VII. Percent changes in the relative site concentrations between a congruent crystal and a crystal vapor phase equilibrated toward stoichiometry. Also included are the percent changes in relative site concentrations between a 0.4 and 2.0 mol % Er:$LiNbO_3$ crystal.

Site number as identified in Ref. 22	Percent change between a vapor phase equilibration treated and an untreated crystal	Percent change between 0.4 and 2.0 mol % Er:$LiNbO_3$
1	+31	−24
2	+4	−7
3	+5	−28
4	−19	+11
5	−22	+16
6	−34	+158

equilibration is shown in Table VII. The most striking result is ~30% reduction in the relative proportion of Er cluster sites (sites 5 and 6) as a result of the equilibration. The observed increase in absorption is attributed to the redistribution of Er sites as a result of the vapor phase equilibration. This redistribution is caused by a change in the defect populations which compensate for the Er incorporation. The simultaneous increase in absorption and decrease in cluster sites indicate that the cluster sites have a smaller cross section than the single ion sites. From an applications perspective, these results are interesting because a reduction in the cluster population not only reduces upconversion in the crystal (which is undesirable for applications such as Er based optical amplification at 1.5 μm) but also increases the amount of light absorbed by the crystal.

The change in the relative proportion of Er_{Nb} and Er_{Li} sites was also determined for the vapor phase equilibrated crystal and the results are shown in Table VI. The data shows an increase in the relative concentration of the 1&2 site group after vapor phase equilibration toward stoichiometry. Comparison to the modeling calculations suggest assigning the 1&2 site group to Er_{Nb}. This assignment is consistent with those from Sec. IV D. In addition, the data show that increasing the Er concentration and increasing the Li_2O content have opposite effects on the relative Er site distribution (Table VII), as predicted by our model. Therefore, we conclude that increasing the Er concentration increases the Li_2O deficiency in $LiNbO_3$ crystals. One way to independently check this conclusion would be to look for the types of defect structures found in Li_2O deficient $LiNbO_3$ and Ti diffused $LiNbO_3$.[38] These structures are thought to be associated with an increase in V_{Nb} and Nb_{Li} defects.[38] An increase in V_{Nb} and Nb_{Li} defects is also predicted by our model calculations (Tables IVa–IVc).

V. CONCLUSIONS

The determination of site redistributions in rare-earth-doped $LiNbO_3$ is facilitated by the use of site-selective spectroscopy. The demonstration of materials engineering in rare-earth-doped $LiNbO_3$ was presented via changes in the Li/Nb stoichiometry. The site redistribution associated with an increase in Er concentration is very similar to that associated with an increase in Li deficiency. Therefore, we conclude that increasing the dopant concentration tends to increase the Li deficiency in the crystal. Our simple model calculations agree with these experimental results. Bringing a 1.0 mol % Er:$LiNbO_3$ crystal closer to stoichiometry, i.e., reducing its Li_2O deficiency, not only reduces the cluster site concentration (~30%) but also increases the absorption of light by the crystal. This behavior indicates that the transition cross section of the Er is larger in the nonclustered sites.

Our results may also have implications for other doped $LiNbO_3$ materials. For example, difficulty has been reported in the Czochralski growth of codoped Nd:MgO:$LiNbO_3$. The formation of striations in boules with high Nd concentrations has limited the amount of Nd that can be incorporated into these crystals.[43] The fact that high Er concentrations in $LiNbO_3$ increases Li_2O deficiency may indicate that Li_2O deficiency is the source of these striations. Altering melt concentrations and/or post growth vapor phase equilibration may therefore be useful for enhancing the quality of these crystals. The Li/Nb ratio can also significantly effect the photorefractive effect,[44] ion diffusivity,[28] dopant solubility,[25] and the Curie temperature[28] in $LiNbO_3$. Therefore, we feel that vapor phase equilibration may be a potentially useful processing technique for the optimization of rare-earth-doped $LiNbO_3$ devices.

ACKNOWLEDGMENTS

The authors would like to acknowledge support by NSF Grants No. ECS9204852 and No. DMR-9305849, and the Newport corporation in the form of the Newport Research Award.

[1] See, for example, S. Koroty and C. Alferness, *Integrated Optical Circuits and Components*, edited by L. Hutcheson (Marcel Dekker, New York, 1987), p. 190.
[2] G. A. Magel, M. M. Fejer, and R. L. Byer, Appl. Phys. Lett. **56**, 108 (1990).
[3] M. Yamada, N. Nada, M. Saitoh, and K. Watanabe, Appl. Phys. Lett. **62**, 435 (1993).
[4] S. K. Korotky and J. J. Veselka, Appl. Phys. Lett. **50**, 1631 (1987).
[5] P. J. Duthie and M. J. Wale, Electron. Lett. **27**, 1265 (1991).
[6] A. Cordova-Plaza, T. Y. Fan, M. J. F. Digonnet, R. L. Byer, and H. J. Shaw, Opt. Lett. **13**, 209 (1988).
[7] E. Lallier, J. P. Pocholle, M. Papuchon, M. de Micheli, M. J. Li, Q. He, D. B. Ostrowsky, C. Grezes-Besset, and E. Pelletier, Opt. Lett. **15**, 682 (1990).
[8] M. Haruna, H. Sewai, H. Nishihara, S. Ikunishi, T. Gozen, and H. Tanaka, Electron. Lett. **30**, 412 (1994).
[9] R. Brinkmann, W. Sohler, and H. Suche, Electron. Lett. **27**, 415 (1991).
[10] S. Helmfrid, G. Arvidsson, J. Webjorn, M. Linnarsson, and T. Pihl, Electron. Lett. **27**, 913 (1991).
[11] T. Y. Fan, A. Cordova-Plaza, M. J. F. Digonnet, R. L. Byer, and H.

J. Shaw, J. Opt. Soc. Am. B **3**, 140 (1986).
[12] H. Suche, L. Baumann, D. Hiller, and W. Sohler, Electron. Lett. **29**, 1111 (1993).
[13] R. Brinkmann, M. Dinand, I. Baumann, Ch. Harizi, W. Sohler, and H. Suche, IEEE Phot. Lett. **6**, 519 (1994).
[14] E. Lallier, J. P. Pocholle, M. Papuchon, Q. He, M. de Micheli, D. B. Ostrowsky, C. Grezes-Besset, and E. Pelletier, Electron. Lett. **27**, 936 (1991).
[15] E. Lallier, D. Papillon, J. P. Pocholle, M. Papuchon, M. de Micheli, and D. B. Ostrowsky, Electron. Lett. **29**, 175 (1993).
[16] B. J. Ainalie, J. Lightwave Technol. **9**, 220 (1991).
[17] D. M. Gill, A. Judy, L. McCaughan, and J. C. Wright, Appl. Phys. Lett. **60**, 1067 (1992).
[18] C. H. Huang, L. McCaughan, and D. M. Gill, J. Lightwave Technol. **12**, 803 (1994).
[19] K. M. Cirillo-Penn and J. C. Wright, Phys. Rev. B **41**, 10 799 (1990).
[20] D. S. Moore and J. C. Wright, J. Chem. Phys. **74**, 1626 (1981).
[21] J. C. Wright, in *Modern Fluorescence*, edited by E. L. Wehry (Plenum, New York, 1981).
[22] D. M. Gill, J. C. Wright, and L. McCaughan, Appl. Phys. Lett. **64**, 2483 (1994).
[23] J. E. Munoz, B. Macalik, and J. Garcia-Sole, Phys. Rev. B **47**, 88 (1993).
[24] J. O. Tocho, E. Camarillo, F. Cusso, F. Jaque, and J. Garcia-Sole, Solid State Commun. **80**, 575 (1991).
[25] B. Macalik, L. E. Bausa, J. Garcia-Sole, and F. Jaque, Appl. Phys. Lett. **62**, 1887 (1993).
[26] R. L. Holman, Ferroelectrics **10**, 185 (1976).
[27] R. C. Alferness, IEEE J. Quantum Electron. **QE-17**, 946 (1981).
[28] R. J. Holmes and D. M. Smyth, J. Appl. Phys. **55**, 3531 (1984).
[29] R. Buisson and J. C. Vial, J. Phys. (Paris) Lett. **42**, L115 (1981).
[30] A. A. Ballman, J. Am. Ceram. Soc. **48**, 112 (1965).
[31] K. Chow, H. G. McKnight, and L. R. Rothrock, Mater. Res. Bull. **9**, 1064 (1974).
[32] S. C. Abrahams and P. Marsh, Acta Crystallogr. B **42**, 61 (1986).
[33] F. A. Kroger and H. J. Vink, in *Solid State Physics: Advances in Research and Applications*, edited by F. Seitz and D. Turnbull (Academic, New York, 1956), Vol. 3.
[34] G. E. Peterson and A. Carnevale, J. Chem. Phys. **56**, 4848 (1972).
[35] H. Donnerberg, S. M. Tomlinson, C. R. A. Catlow, and O. F. Schirmer, Phys. Rev. B **40**, 11 909 (1989).
[36] H. J. Donnerberg, S. M. Tomlinson, and C. R. A. Catlow, J. Phys. Chem. Solids **52**, 201 (1991).
[37] H. Donnerberg, S. M. Tomlinson, C. R. A. Catlow, and O. F. Schimer, Phys. Rev. B **44**, 4877 (1991).
[38] M. E. Twigg, D. M. Maher, S. Nakahara, T. T. Sheng, and R. J. Holmes, Appl. Phys. Lett. **50**, 501 (1987).
[39] L. Rebouta, J. C. Soares, M. F. da Silva, J. A. Sanz-Garcia, E. Dieguez, and F. Agullo-Lopez, Appl. Phys. Lett. **55**, 120 (1989).
[40] Qi-Ren Zhang and Xi-Qi Feng, Phys. Rev. B **43**, 12 019 (1991).
[41] I. P. Kaminlow and J. R. Carruthers, Appl. Phys. Lett. **22**, 326 (1973).
[42] A. J. Ramponi and J. C. Wright, Phys. Rev. B **35**, 2413 (1987).
[43] Norman Sanford (unpublished).
[44] R. L. Holman, P. J. Cressman, and J. F. Revelli, Appl. Phys. Lett. **32**, 280 (1978).